Diffractive Dijet Electroproduction at HERA

H1 Collaboration

Abstract

The production of high transverse momentum jet pairs as components of the dissociating photon system X in the diffractive deep-inelastic scattering process $ep \rightarrow eXY$ is studied, where the system Y is dominantly a proton and the squared four momentum transferred at the proton vertex is small. In a factorisable partonic pomeron model, the data suggest that the pomeron parton distributions are heavily dominated by gluons, with substantial contributions at all fractional momenta. The measured overall dijet rates and differential cross sections are generally well described by a model based on pomeron parton distributions determined from a QCD analysis of the diffractive structure function $F_2^{D(3)}(\beta, Q^2, x_{I\!P})$. This supports the hypothesis that universal pomeron parton densities can be used to describe different hard scattering processes in diffractive DIS. Viewed in terms of the diffractive scattering of partonic fluctuations of the photon, the data are dominated by photon Fock states of higher multiplicity than a simple $q\bar{q}$ pair.

1 Introduction

1.1 Diffractive Scattering at HERA

Deep-inelastic scattering (DIS) events at HERA containing large gaps in the pseudorapidity distribution of final state hadrons have dominantly been ascribed to a diffractive production mechanism [1]. They thus provide an opportunity to illucidate the parton dynamics of diffractive scattering and the partonic structure of the diffractive exchange or *pomeron*.

The generic diffractive process at HERA of the type $ep \rightarrow eXY$ is illustrated in figure 1(a). A photon of virtuality Q^2 interacts with a proton at a $\gamma^* p$ invariant mass W with squared four momentum transfer t to produce distinct final state hadronic systems X and Y of invariant masses M_{X} and M_{Y}. With q, p and p_{Y} denoting the four vectors of the photon, proton and final state system Y respectively, the variables

$$x_{I\!P} = \frac{q.(p - p_{\mathrm{Y}})}{q.p} \simeq \frac{M_{\mathrm{X}}^2 + Q^2}{W^2 + Q^2} \tag{1}$$

$$\beta = \frac{Q^2}{2q.(p - p_{\mathrm{Y}})} \simeq \frac{Q^2}{M_{\mathrm{X}}^2 + Q^2} \tag{2}$$

are usually introduced. In the proton infinite momentum frame, $x_{I\!P}$ is the fraction of the proton momentum that is exchanged to the system X and β is the fraction of the exchanged momentum carried by the quark coupling to the photon.
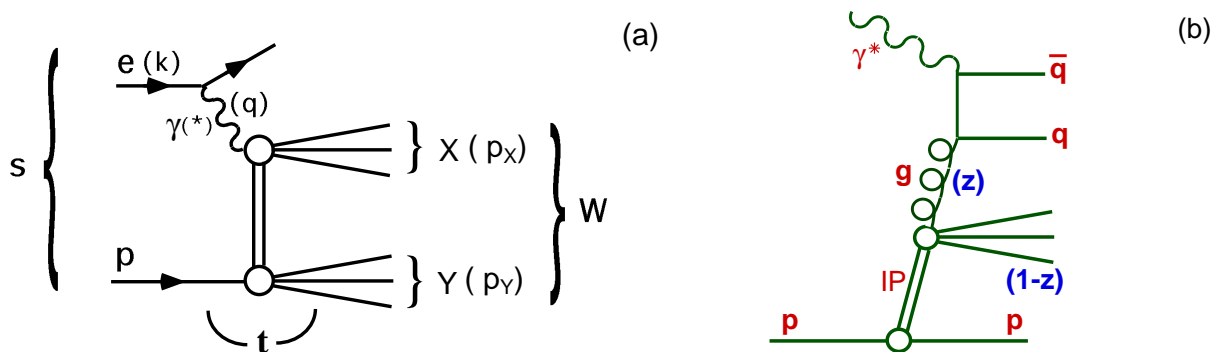

Figure 1: (a) The generic diffractive process at HERA, where a photon interacts with a proton via a net colour singlet exchange, producing final state hadronic systems X and Y. Where the masses of X and Y are small, the two systems are separated by a large gap in rapidity. (b) Diagram of the dominating leading order QCD process in models in which the pomeron has partonic sub-structure. A $q\bar{q}$ pair is produced via photon-gluon-fusion ($\gamma^* g \rightarrow q\bar{q}$).

1.2 Theoretical Perspective

The diffractive DIS cross section can be expressed in terms of convolutions of parton cross sections with *diffractive parton distributions* [2, 3], expressing proton parton probability distributions under the additional constraint of an intact final state proton with particular values

1

of $x_{I\!P}$ and t. The phenomenology of soft hadronic interactions suggests that is is possible to introduce a universal pomeron exchange with a flux factor dependent only on $x_{I\!P}$ and t. With the assumption of a factorisable partonic pomeron exchange, the framework of diffractive parton distributions can be used to define parton distributions for the pomeron [4], which should describe all hard diffractive scattering processes. The QCD evolution of the pomeron parton distributions should then obey the DGLAP equations, β and Q^2 being the relevant variables for evolution [5].

An alternative approach to diffractive DIS, avoiding the assumption of a factorisable pomeron, is to attempt to describe the process from first principles of QCD with a knowledge of the parton distributions of the proton. It is informative to think of the process in the proton rest frame, where a photon splitting $\gamma^* \to q\bar{q}$ takes place well in advance of the target. The $q\bar{q}$ system may or may not develop into a higher multiplicity partonic system (e.g. $q\bar{q}g$) before interacting diffractively with the proton. Many properties of the diffractive final state (in particular the β distribution [6]) can be deduced from a knowledge of the partonic wavefunctions of the photon alone. However, a model for the diffractive interaction of the partonic photon fluctuations with the proton is still required for a full description. The simplest realisation of a net colour singlet exchange at the parton level is a pair of gluons with opposite colour charges [7]. Approaches based on the exchange of gluon pairs can be found in [6,8–10]. Recent calculations of the expected jet production rates for both the $q\bar{q}$ [9] and $q\bar{q}g$ [10] photon fluctuations have been implemented in Monte Carlo models, allowing hadron level predictions to be made. An alternative semi-classical approach has been developed,[1] based on partonic scattering from the average colour field of the proton [11], with those final state partonic systems that emerge in a net colour singlet state contributing to the diffractive cross section.

1.3 Pomeron Parton Distributions

Measurements of the total cross section for diffractive deep-inelastic scattering, usually presented in the form of a diffractive structure function $F_2^{D(3)}(\beta, Q^2, x_{I\!P})$ [13,14], have shown that, to the present level of accuracy, the Regge factorisation property of [4] is obeyed. Pomeron parton distributions have been extracted from QCD analyses of $F_2^{D(3)}$ measurements. The data are found to require the dominance of gluons in the exchange, carrying between 80% and 90% of the total momentum of the pomeron [13]. Figure 1(b) then represents the dominant process at leading order of QCD. A gluon carrying a fraction $z_{I\!P}$ of the exchanged momentum undergoes boson-gluon fusion with the virtual photon ($\gamma^* g \to q\bar{q}$). Gluon distributions extracted from $F_2^{D(3)}$ data contain significant contributions in the region of high $z_{I\!P}$ at low factorisation scales. However, the detailed shape and normalisation of the gluon distribution is not yet well constrained by inclusive measurements of diffractive DIS, since it is only indirectly determined from the scaling violations. Measurements of exclusive final states such as those containing dijets or charm represent a promising means of obtaining a better understanding of the gluon distribution of the pomeron.

Here, we compare two sets of gluon dominated pomeron parton distributions, extracted in a QCD analysis of H1 1994 $F_2^{D(3)}$ data [13], with diffractive dijet cross section measurements. In

---

[1]It has been demonstrated [12] that the semi-classical model can be re-expressed in the form of diffractive parton distributions.

the first set (fit 2 in [13], described as the 'flat' gluon here), the gluon density is relatively flat in $z_{I\!P}$ at low factorisation scales. In the second (fit 3 in [13], described as the 'peaked' gluon here), the gluon distribution at low scales is peaked at large $z_{I\!P}$. Both sets of parton distributions have been found to give a good description of data on many properties of the hadronic final state in diffractive DIS [15–17].[2]

1.4 Diffractive Dijet Production

Since the dominant boson-gluon fusion process naturally leads to two jet final states, diffractive dijet cross sections are particularly sensitive to the role of gluons in diffraction. Dijet production directly probes the gluon content of the pomeron in a manner that is not possible in inclusive measurements.

A hadron level estimator, $z_{I\!P}^{\rm jets}$ of the fraction $z_{I\!P}$ of the pomeron momentum that enters the hard scattering process can be defined as

$$
z_{I\!P}^{\rm jets} = \frac{M_{12}^2 + Q^2}{M_{\rm X}^2 + Q^2} \; , \tag{3}
$$

where M_{12}^2 is the squared invariant mass of the dijet system. In [17], it was shown that the rates and $z_{I\!P}^{\rm jets}$ distributions of dijets produced in diffractive DIS are well described by Monte Carlo models based on the parton distributions extracted from QCD analysis of $F_2^{D(3)}$, the 'flat' gluon distribution giving a slightly better description than the 'peaked' gluon distribution. In this paper, new H1 measurements of dijets in diffractive DIS are presented, providing improved constraints on the pomeron gluon density.

2 Data Selection

Data taken with the H1 detector in 1996 are used for the analysis.[3] The integrated luminosity of the sample is $5.0 \ {\rm pb}^{-1}$. With this increased luminosity and reductions in the minimum jet transverse momentum and minimum Q^2 requirements, the total dijet sample analysed is a factor of approximately 12 larger than that used in our previous measurement [17], thus improving the precision considerably. The kinematic constraint imposed by requiring two high transverse momentum jets implies that the data probe the region of large $M_{\rm X}$ and hence low β (see equation 2). The β range of the dijet data ($0.003 \lesssim \beta \lesssim 0.3$, see figure 2) extends to values lower than those for which $F_2^{D(3)}$ was measured in [13].

---

[2]A recent measurement of diffractive charm production [18] represents the first indication of deviations from this picture.

[3]A detailed description of the H1 detector can be found elsewhere [19].

2.1 Inclusive DIS Selection

Events are triggered on the basis of a high energy electromagnetic cluster in the backward Spaghetti calorimeter (SPACAL), a reconstructed vertex and a high transverse momentum track in the central tracking chambers.

An inclusive DIS sample in which the final state positron is detected and measured in the SPACAL is obtained using standard selection criteria [20]. Data from inefficient regions of the SPACAL and run periods in which essential components of the detector were inoperational are rejected. To remove background from non-ep interactions, a reconstructed event vertex is required in the region $-30 < z_{\mathrm{vtx}} < 30$ cm. To reduce the contribution from events with initial state QED radiation, the total[4] $E - p_z$ of all reconstructed final state particles, including the electron, is required to be greater than 35 GeV. The inclusive kinematic variables y and Q^2 are calculated using the electron energy and angle measurements.

2.2 Selection of Diffractive Events

A sample of diffractive events is obtained on the basis of an absence of hadron production in a large region around the outgoing proton direction. A rapidity gap is identified by requiring a lack of activity in the more forward components of the H1 detector. It is demanded that there should be no activity above expected noise levels in the proton remnant tagger, a series of scintillator sheets surrounding the beamline at $z = 26$ m, and the forward muon detector, a set of drift chambers that are sensitive to hadronic activity at large rapidity due to secondary scattering of particles from the beam-pipe and surrounding material. These selection criteria ensure that the proton either remains intact with $|t| \lesssim 1$ GeV^2 or dissociates to a low mass system of $M_Y \lesssim 1.6$ GeV. In addition, it is required that there should be no significant activity in the main liquid argon calorimeter forward of a pseudorapidity $\eta = 3.2$. This ensures that diffractive events at low $x_{I\!P}$ are selected. The hadronic final state is reconstructed using a method that combines tracks and calorimeter clusters without double counting [21]. An explicit cut $x_{I\!P} \lesssim 0.05$ is applied, where $x_{I\!P}$ is calculated using equation 1.

2.3 Selection of Dijet Events

A CDFCONE [22] jet algorithm of unit cone radius is performed on all hadronic final state objects in the centre of mass frame of the $\gamma^* p$ system. Exactly two jets are required in the laboratory pseudorapidity range $-1.0 < \eta_{\mathrm{lab}}^{\mathrm{jet}} < 2.2$, with transverse momentum $p_{\mathrm{T,jet}} > 4$ GeV relative to the $\gamma^* p$ collision axis. The selected events display clear jet-like structures with the two jets dominantly back-to-back in azimuth.

The measurement is restricted to a kinematic region in which the acceptance is large and approximately constant. The full kinematic region in which the measurements are made and to which the final cross sections are corrected is specified in table 1.

---

[4] The H1 coordinate system is such that the $+z$ direction is that of the outgoing proton beam.

4

Kinematic Domain of Measurement
$4 < Q^2 < 80$ GeV^2
$0.1 < y < 0.7$
$x_{I\!P} < 0.05$
$M_{Y} < 1.6$ GeV
$|t| < 1$ GeV^2
$N_{\mathrm{jets}} = 2$
$p_{\mathrm{T,jet}} > 4$ GeV

Table 1: The full kinematic range in which the dijet production cross sections are measured. Note that there is no explicit restriction on $\eta^{\mathrm{jet}}_{\mathrm{lab}}$.

3 Cross Section Measurement

3.1 Trigger Efficiency and Acceptance Corrections

Cross sections are measured differentially in Q^2, $p_{\mathrm{T,jet}}$, $x_{I\!P}$, $z^{\mathrm{jets}}_{I\!P}$ and $\langle \eta \rangle^{\mathrm{jet}}_{\mathrm{lab}}$, where the last variable is the average laboratory pseudorapidity of the two jets. The efficiency of each component of the trigger used is evaluated using data taken with independent triggers. The main losses come from the track requirement of the trigger, which is between 80% and 90% efficient in the measured region. The data are corrected for this effect using a parameterisation as a function of M_{X}.

The data are corrected for acceptance and migrations due to the finite resolution of the reconstruction using iterative unfolding procedures [23] based on the RAPGAP [24] Monte Carlo event generator version 2.08/01, interfaced to a detailed simulation of the H1 detector. RAPGAP models the region $x_{I\!P} < 0.2$ for processes in which the proton remains intact. Diffractive interactions are simulated by assuming a factorisable pomeron exchange, the flux of which takes a Regge motivated form proportional to $(1/x_{I\!P})^{2\alpha_{I\!P}(t)-1} e^{b_{I\!P}t}$ with pomeron trajectory $\alpha_{I\!P}(t) = 1.20 \pm 0.26t$ and slope parameter $b_{I\!P} = 4.6$ GeV^{-2} [13]. The electron-pomeron interaction cross section is obtained from hard scattering matrix elements up to leading order of QCD, convoluted with parton distributions for the pomeron at a momentum fraction $z_{I\!P}$ and factorisation scale $\mu^2 = Q^2$. The pomeron parton distributions are taken from the 'flat' gluon parameterisation described in section 1.3. A small contribution from a sub-leading exchange is also included in the simulation as described in [17]. Higher order effects in the QCD cascade are simulated using parton showers [25].

The Monte Carlo model gives a good description of the data distributions in all relevant quantities. Some example control distributions are shown in figure 2. The acceptance correction factors applied to the data are always less than a factor of three. The purities and stabilities of all bins are in excess of 30 % according to the Monte Carlo simulations.

3.2 Further Corrections to the Data

In addition to the basic acceptance correction described in section 3.1, several other small corrections have to be taken into account:

- Smearing from the region $x_{I\!P} > 0.2$ or $M_Y > 5$ GeV is estimated using the RAPGAP model of inclusive DIS processes. Corrections of up to 8% are applied.

- The DIFFVM Monte Carlo model [26], which simulates both elastic and proton dissociative vector meson production, is used to study the migrations across the kinematic boundary of the measurement, $M_Y = 1.6$ GeV. The resulting correction factor is 1.024 ± 0.050.

- Fluctuations in the noise levels in the forward detectors can result in the non-selection of diffractive events. These losses have been quantified by studying a sample of random read-outs of the detector, not correlated with ep interactions. All cross sections are corrected by a constant factor of 1.08 ± 0.02 to account for this effect.

- QED radiative corrections have been evaluated using an interface to the HERACLES program [27] and are typically at the level of 5%.

Contamination from interactions of the beams with residual gas in the beam-pipe and from photoproduction interactions in which a hadron fakes an electron signal have been found to be negligible.

3.3 Systematic Error Analysis

Systematic errors arise from the following sources:

- Uncertainties in the calibration of various detector components (calorimeter energy scales, track resolution, uncertainties in the electron energy and polar angle measurements and forward detector efficiencies). When combined in quadrature, these uncertainties are typically at the level of 12%.

- The model dependence of the acceptance corrections is estimated by varying the $x_{I\!P}$, t, $z_{I\!P}$ and p_T distributions in the RAPGAP Monte Carlo model used for the unfolding. The ratio of proton dissociation to proton elastic processes and the M_Y distribution for proton dissociation are varied in the DIFFVM model used to estimate the migrations about $M_Y = 1.6$ GeV. In addition, the corrections due to migrations from the regions $x_{I\!P} > 0.2$ and $M_Y > 5$ GeV are varied by $\pm 100\%$. The combined systematic error from these effects is at the level of 9%.

- Uncertainties in the luminosity determination, trigger efficiency, noise contamination in the forward detectors and radiative corrections lead to further systematic errors at the level of 12%.

The overall systematic error is evaluated for each data point presented and added in quadrature with the statistical error to obtain the total uncertainties. The systematic uncertainties give the larger contribution to the errors on most data points.

4 Results

4.1 Overall Dijet Rates

The cross sections corrected to the Born level are shown differentially in the two important scales in the process, $p_{\mathrm{T,jet}}$ and Q^2 in figure 3. Here $p_{\mathrm{T,jet}}$ is the mean transverse momentum of the two hadron level jets relative to the $\gamma^* p$ collision axis in the hadronic centre of mass frame.

Here and elsewhere, the data are compared with the predictions of the RAPGAP model based on the diffractive parton distributions extracted from $F_2^{D(3)}$. In this model, approximately 75% of dijet events in the kinematic region studied are attributable to the boson gluon fusion process from the pomeron gluon distribution. The model used contains only the simplest assumptions on the implementation of the pomeron parton distributions. No attempt has yet been made to investigate the possible effects of interference between the pomeron and sub-leading exchanges, found to be possible in [13], or the possibility of intrinsic transverse momentum of the pomeron partons [28]. The effects of resolved virtual photon interactions [29], which may be important since $p_{\mathrm{T,jet}}^2 > Q^2$ for most of the data, have also yet to be studied.

Both differential cross sections shown in figure 3 are well described by the RAPGAP model with a 'flat' gluon distribution at low scales (fit 2). Similarly good descriptions are obtained when the 'peaked' gluon parton distributions are used instead. There is little sensitivity in these distributions to the appropriate choice of factorisation scale, with both $\mu^2 = Q^2 + p_{\mathrm{T}}^2$ and $\mu^2 = Q^2$ giving a reasonable description of the data in both shape and normalisation.

4.2 Dependence on $x_{I\!P}$ and Jet Pseudorapidity

The cross section is shown differentially in $x_{I\!P}$ and $\langle \eta \rangle_{\mathrm{jets}}^{\mathrm{lab}}$ in figure 4, where $\langle \eta \rangle_{\mathrm{jets}}^{\mathrm{lab}}$ is the mean pseudorapidity of the two jets in the laboratory frame. The rising structure of the cross section differential in $x_{I\!P}$ reflects the kinematic constraint imposed by the requirement of a pair of jets each with $p_{\mathrm{T,jet}} > 4$ GeV. This implies that $M_{\mathrm{X}} > 8$ GeV and in turn suppresses the cross section in the low $x_{I\!P}$ region (see equation 1).

In figure 4 (top), the contribution in the simulation from the sub-leading exchange is shown. As expected, this contribution is significant only at large $x_{I\!P}$. However, even at the largest $x_{I\!P}$, the pomeron contribution is dominant. This can be understood from the large gluon distribution of the pomeron and the fact that the boson-gluon fusion process naturally leads to a two jet final state. For the sub-leading exchange, quark initiated interactions play a much more important role. The dominant process is then $\gamma^* q \to q$, which rarely leads to high transverse momentum jets.

The RAPGAP Monte Carlo model gives a reasonable description of the $x_{I\!P}$ and $\langle \eta \rangle_{\mathrm{jets}}^{\mathrm{lab}}$ distributions, though when viewed in fine detail, there are some discrepancies. In particular, the predicted cross section is smaller than that measured at the largest $x_{I\!P}$ and the data are on average at larger pseudorapidity (more inclined towards the outgoing proton direction) than the model predicts. These discrepancies between data and simulation are also reflected in the $z_{I\!P}^{\mathrm{jets}}$ distribution (see figures 6 and 7), where there is an excess of data over the predictions at low

7

$z_{I\!P}^{\rm jets}$. This corresponds largely to the very low β region that was not measured in [13] and hence was not considered in the QCD analysis used to extract the pomeron parton distributions. It is therefore likely that modifications to the gluon distribution at low $z_{I\!P}$ may restore a good description of the dijet measurements in this region without affecting the description of the $F_2^{D(3)}$.

4.3   Dependence on Fractional Momentum of the Diffractive Exchange

An observable in diffractive dijet production that is highly sensitive to the underlying parton dynamics is the ratio of the invariant mass M_{12} of the jet pair to that of the total diffractively produced system, $M_{\rm X}$. Scatter plots of $M_{\rm X}^2$ versus M_{12}^2 are shown for the uncorrected data sample and the RAPGAP simulation in figure 5. It is clear that M_{12}^2 is usually much smaller than $M_{\rm X}^2$, implying that the system X generally contains many hadrons that are not associated with the jets. This has major implications in all models of diffractive DIS, which are discussed below in the context of corrected cross sections differential in the hadron level pomeron momentum fraction estimator $z_{I\!P}^{\rm jets}$.

In figure 6, the dijet cross sections are shown differentially in $z_{I\!P}^{\rm jets}$. Although there are contributions throughout the measured range, it is clear that the cross section is largest at medium or small $z_{I\!P}^{\rm jets}$. In a partonic pomeron model, this implies that the fraction of the pomeron momentum transferred to the dijet system is generally less than unity. Even allowing for leakage from the jets of hadrons associated with the partons emerging from the hard scattering,[5] this suggests that the fraction of the pomeron momentum carried by the parton entering the hard scattering is usually rather small.

The data in figure 6 are compared to the RAPGAP model with different assumptions for the parton distributions of the pomeron and the factorisation scale. Except at the lowest $z_{I\!P}^{\rm jets}$, the data are reasonably well described by all of the models. In the case of the 'peaked' gluon model, a better description is obtained in the high $z_{I\!P}^{\rm jets}$ region when the factorisation scale $\mu^2 = Q^2 + p_{\rm T}^2$ is used than is the case for $\mu^2 = Q^2$. Since $Q^2 < p_{\rm T,jet}^2$ for most of the data under consideration, Q^2 is not expected to be the most appropriate choice of scale.

In models based on the diffractive scattering of partonic fluctuations of the photon from the proton, the entire momentum of the diffractive exchange is transferred to the dijet system in the case of the $q\bar{q}$ Fock state. The $q\bar{q}$ fluctuation is thus expected to contribute only near $z_{I\!P}^{\rm jets} = 1$ [17], The dominance of lower values of $z_{I\!P}^{\rm jets}$ in the data implies that $q\bar{q}g$ or higher multiplicity Fock states play the most important role in the high transverse momentum dijet production process. This dominance of photon fluctuations involving one or more gluons has been predicted for the low β region of the present data on the basis of fits to $F_2^{D(3)}$ which aim to decompose the data into different photon Fock states [6].

Figure 7 shows the overall $z_{I\!P}^{\rm jets}$ distribution in the restricted kinematical region $12 < Q^2 < 80 \;\mathrm{GeV}$ together with the decomposition of the RAPGAP prediction into different contributions from the pomeron and the sub-leading exchange. As already noted, the contribution from the sub-leading exchange is small. The quarks from the pomeron parton distributions also lead to

---

[5]The correlation between the parton level variable $z_{I\!P}$ and the hadron level variable $z_{I\!P}^{\rm jets}$ was discussed in [17].

only a small fraction of the dijet cross section (dominantly through the QCD-Compton process). Since the pomeron and sub-leading exchange quark distributions are rather well constrained by $F_2^{D(3)}$ measurements, it is reasonable to ascribe the remainder of the dijet cross section to gluon initiated processes. Approximately 75% of the dijet data are then attributable to gluons. The RAPGAP model prediction for the gluon contribution, based on the scaling violations of $F_2^{D(3)}$, is in remarkably good agreement with the dijet data.

These new measurements thus confirm our earlier conclusions from diffractive dijet data [17] that a large fraction of gluons is required in the pomeron parton distributions and that the dijet rates can be reproduced using parton distributions extracted from QCD analysis of $F_2^{D(3)}$ with relatively simple assumptions. Similar conclusions have been reached from studies of several other properties of the hadronic final state in diffractive DIS [15, 16].

Figures 8 and 9 show the cross section differential in $z_{I\!\!P}^{\mathrm{jets}}$ divided into two regions of the two scales in the problem, Q^2 and $p_{\mathrm{T,jet}}^2$. Except for the data points at the lowest $z_{I\!\!P}^{\mathrm{jets}}$, the data are acceptably described by the RAPGAP simulation. The differential cross sections are very similar in shape for the two Q^2 regions. The data in two bins of $p_{\mathrm{T,jet}}^2$ differ in shape. The dominant effect here is kinematical in nature. The large values of M_{12}^2 required at large $p_{\mathrm{T,jet}}^2$, and the relatively small values of M_{X}^2 accessed force the data to larger $z_{I\!\!P}^{\mathrm{jets}}$ than is the case at low $p_{\mathrm{T,jet}}^2$.

5   Conclusions

Dijet production in diffractive DIS has been studied in a wider kinematic region and with much better precision than has previously been possible. Cross sections have been measured differentially in Q^2, $p_{\mathrm{T,jet}}$, $x_{I\!\!P}$, $\langle\eta\rangle_{\mathrm{lab}}^{\mathrm{jets}}$ and $z_{I\!\!P}^{\mathrm{jets}}$. Measurements of the cross section differential in $z_{I\!\!P}^{\mathrm{jets}}$ have also been made in two regions of the scales Q^2 and $p_{\mathrm{T,jet}}^2$.

The overall dijet cross section and most features of the differential cross sections are well described by a partonic pomeron model based on pomeron parton distributions extracted from $F_2^{D(3)}$ measurements in which over 80% of the exchanged momentum is carried by gluons. The dijet measurements directly access the gluon content of the pomeron, in contrast to inclusive diffractive data, from which the gluon distribution can only be inferred from the scaling violations. The $F_2^{D(3)}$ and dijet measurements have very different systematics and require different applications of the pomeron parton distributions. The remarkable agreement between the two analyses thus provides strong support for the hypothesis that a universal set of heavily gluon dominated factorisable parton distributions are applicable to the description of all hard scattering processes in diffractive DIS.

Viewed in terms of the diffractive scattering from the proton of partonic fluctuations of the photon, the dominant contribution in the low β, high transverse momentum region of the data arises from photon Fock states of higher multiplicity than a simple $q\bar{q}$ pair.

Acknowledgements

We are grateful to the HERA machine group whose outstanding efforts have made and continue to make this experiment possible. We thank the engineers and technicians for their work constructing and maintaining the H1 detector, our funding agencies for financial support, the DESY technical staff for continual assistance and the DESY directorate for the hospitality which they extend to the non-DESY members of the collaboration.

References

[1] H1 Collaboration, T. Ahmed et al., Phys. Lett. **B348** (1995) 681.

[2] L. Trentadue, G. Veneziano, Phys. Lett. **B323** (1994) 201.

[3] A. Berera, D. Soper, Phys. Rev. **D50** (1994) 4328.

[4] G. Ingelman, P. Schlein, Phys. Lett. **B 152** (1985) 256.

[5] J. Collins, Phys. Rev. **D57** (1998) 3051.

[6] J. Bartels, J. Ellis, H. Kowalski, M. Wüsthoff, Eur. Phys. J. **C7** (1999) 443.

[7] F. Low, Phys. Rev. **D12** (1975) 163.
    S. Nussinov, Phys. Rev. Lett. **34** (1975) 1286.

[8] A. Mueller, Nucl. Phys. **B335** (1990) 115.
    M. Ryskin, Sov. J. Nucl. Phys. **52** (1990) 529.
    N. Nikolaev, B. Zakharov, Z. Phys. **C53** (1992) 331.
    M. Diehl, Z. Phys. **C66** (1995) 181.

[9] J. Bartels, H. Lotter, M. Wüsthoff, Phys. Lett. **B379** (1996) 239.
    J. Bartels, C. Ewerz, H. Lotter, M. Wüsthoff, Phys. Lett. **B386** (1996) 389.

[10] J. Bartels, H. Jung, M. Wüsthoff, DESY **99-027**, *hep-ph/9903265*.

[11] W. Buchmüller, T. Gehrmann, A. Hebecker, Nucl. Phys. **B537** (1999) 477.

[12] A. Hebecker, Nucl. Phys. **B505** (1997) 349.

[13] H1 Collaboration, C. Adloff et al., Z. Phys. **C76** (1997) 613.

[14] ZEUS Collaboration, J. Breitweg et al., Eur. Phys. J. **C6** (1999) 43.

[15] H1 collaboration, Phys. Lett. **B428** (1998) 206
    ZEUS collaboration, Phys. Lett. **B421** (1998) 368.
    H1 collaboration, Eur. Phys. J. **C1** (1998) 495.
    H1 collaboration, Eur. Phys. J. **C5** (1998) 439.

[16] ZEUS collaboration, Eur. Phys. J. **C5** (1998) 41.

[17] H1 collaboration, Eur. Phys. J. **C6** (1999) 421.

[18] H1 Collaboration, *'Measurement of the Production of $D^{*\pm}$ Mesons in Deep Inelastic Diffractive Interactions at HERA'*, paper 23 submitted to EPS99, Tampere.

[19] H1 Collaboration, I. Abt et al., Nucl. Instr. and Meth. **A386** (1997) 310 and 348.

[20] H1 Collaboration, *'A Measurement of the Inclusive Deep-Inelastic ep Scattering Cross Section at Low Q^2 at HERA'*, Paper 260 submitted to EPS97, Jerusalem.

[21] H1 Collaboration, C. Adloff et al., Z. Phys. **C74** (1997) 221.

[22] CDF Collaboration., F. Abe et al., Phys. Rev. **D45** (1992) 1448.

[23] G. D'Agostini, Nucl. Instr. and Meth. **A362** (1995) 487.

[24] H. Jung, Comp. Phys. Comm. **86** (1995) 147 (version 2.08/01 was used here). See also http://www-h1.desy.de/∼jung/rapgap.html.

[25] M. Bengtsson, T. Sjöstrand, Z. Phys. **C37** (1988) 465.

[26] B. List, *'Diffraktive J/ψ–Produktion in Elektron–Proton–Stößen am Speicherring HERA'*, Diploma Thesis (Tech. Univ. Berlin), 1993 (unpublished).

[27] H. Spiesberger, H. Möhring, Comp. Phys. Comm. **69** (1992) 155.

[28] N. Nikolaev, *'Intrinsic $k_\perp$ in the Pomeron'*, to appear in proceedings of the workshop on Monte Carlo Generators for HERA Physics (http://www.desy.de/∼heramc/).

[29] H1 Collaboration, C. Adloff et al., Phys. Lett. **B415** (1997) 418. H1 Collaboration, C. Adloff et al., DESY **98-205**, submitted to Eur. Phys. J.
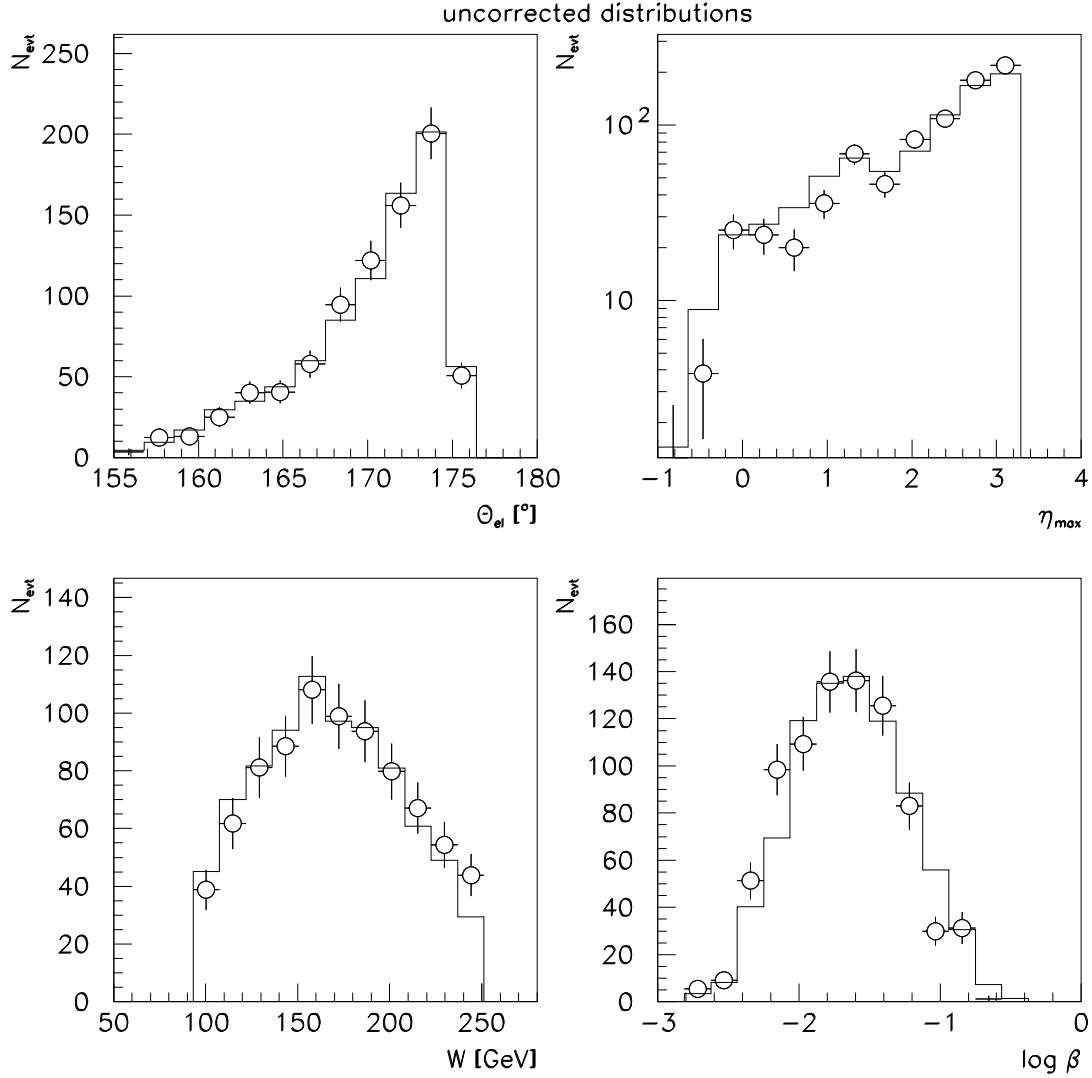
Figure 2: Uncorrected distributions for diffractive dijet data, after all selection cuts have been applied (*data points*), compared with the prediction of a partonic pomeron model as implemented in the RAPGAP event generator (*histogram*). The electron scattering angle θ_{el}, the maximum pseudorapidity η_{max} of final state hadrons observed in the liquid argon calorimeter, the invariant mass of the photon-proton system W and $\beta = Q^2/(Q^2 + M_X^2)$ are shown. The number of events in the Monte Carlo sample has been scaled to match that in the data.
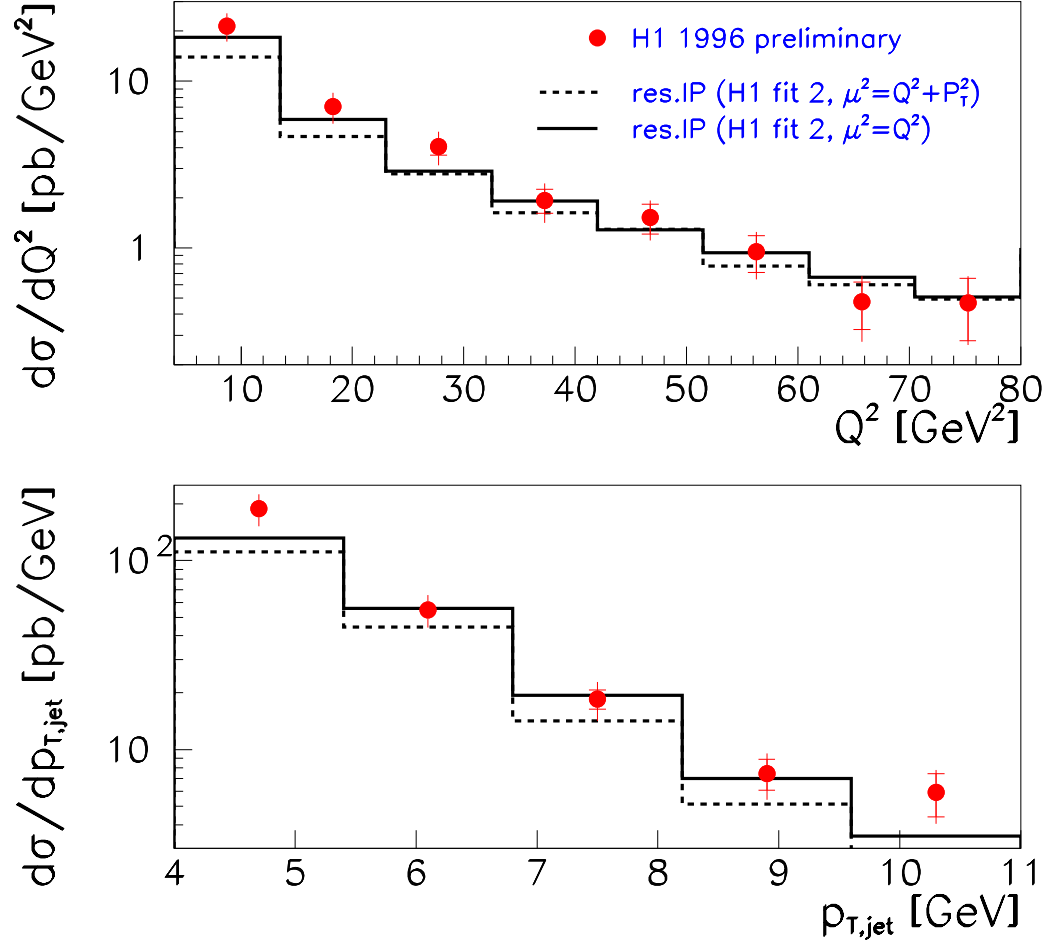
Figure 3: Differential hadron level cross sections for diffractive dijet production as a function of Q^2 and of $p_{T,jet}$. The cross sections are measured in the kinematic range specified in table 1. The inner error bars represent the statistical and the outer error bars the combined statistical and systematical errors. Also shown are the predictions from a partonic pomeron model as implemented in the RAPGAP generator. 'Flat' gluon dominated parton densities are used for the pomeron, obtained from QCD fits to the diffractive structure function $F_2^{D(3)}$ and evolved to scales $\mu^2 = Q^2$ or $\mu^2 = Q^2 + p_T^2$.
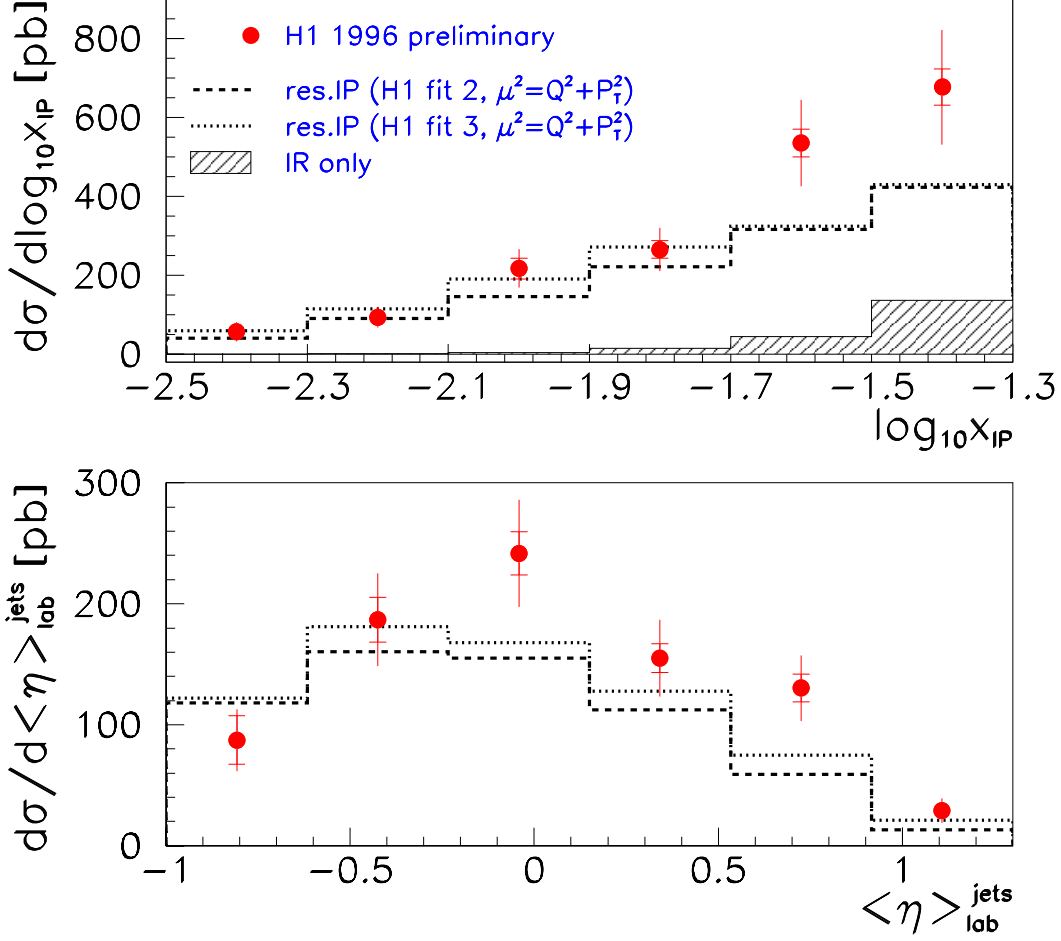
Figure 4: Differential hadron level cross section for diffractive dijet production as a function of $\log x_{I\!P}$ and $\langle\eta\rangle_{\mathrm{lab}}^{\mathrm{jets}}$, the average pseudorapidity of the two hadron level jets in the laboratory frame. The cross sections are measured in the kinematic range specified in table 1. The data are compared to a partonic pomeron model as implemented in the RAPGAP generator, incorporating 'flat' (fit 2) and 'peaked' (fit 3) gluon-dominated parton densities from [13], evolved to a scale $\mu^2 = Q^2 + p_{\mathrm{T}}^2$.
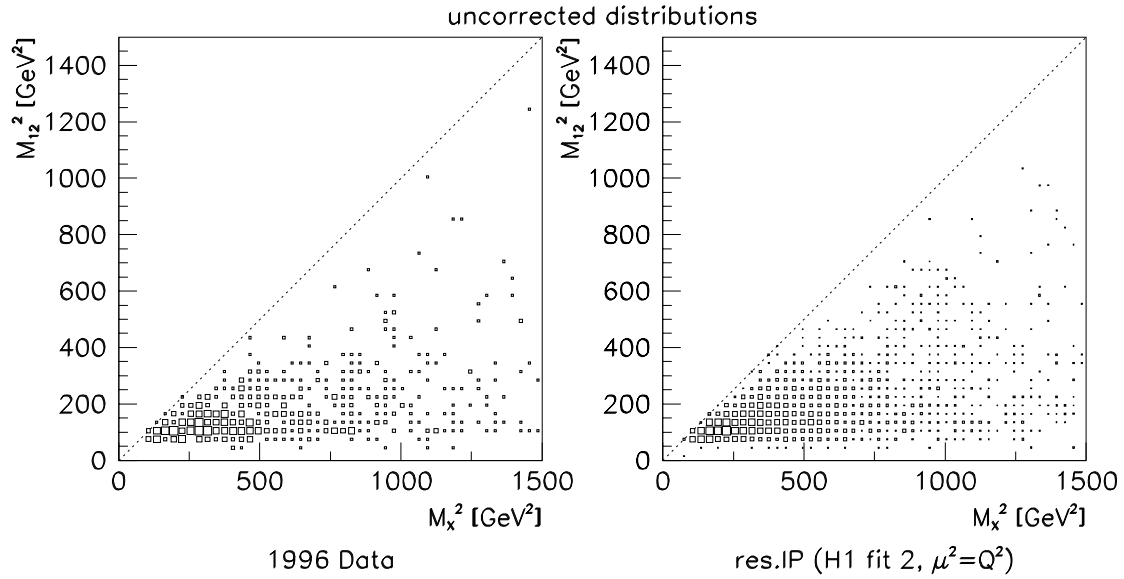
Figure 5: Correlation of the measured squared invariant dijet mass M_{12}^2 with the total squared invariant mass of the diffractively produced system M_X^2. The uncorrected data distribution (left) is compared with a 'flat' gluon dominated partonic pomeron model implemented in the RAPGAP generator with $\mu^2 = Q^2$ (right).
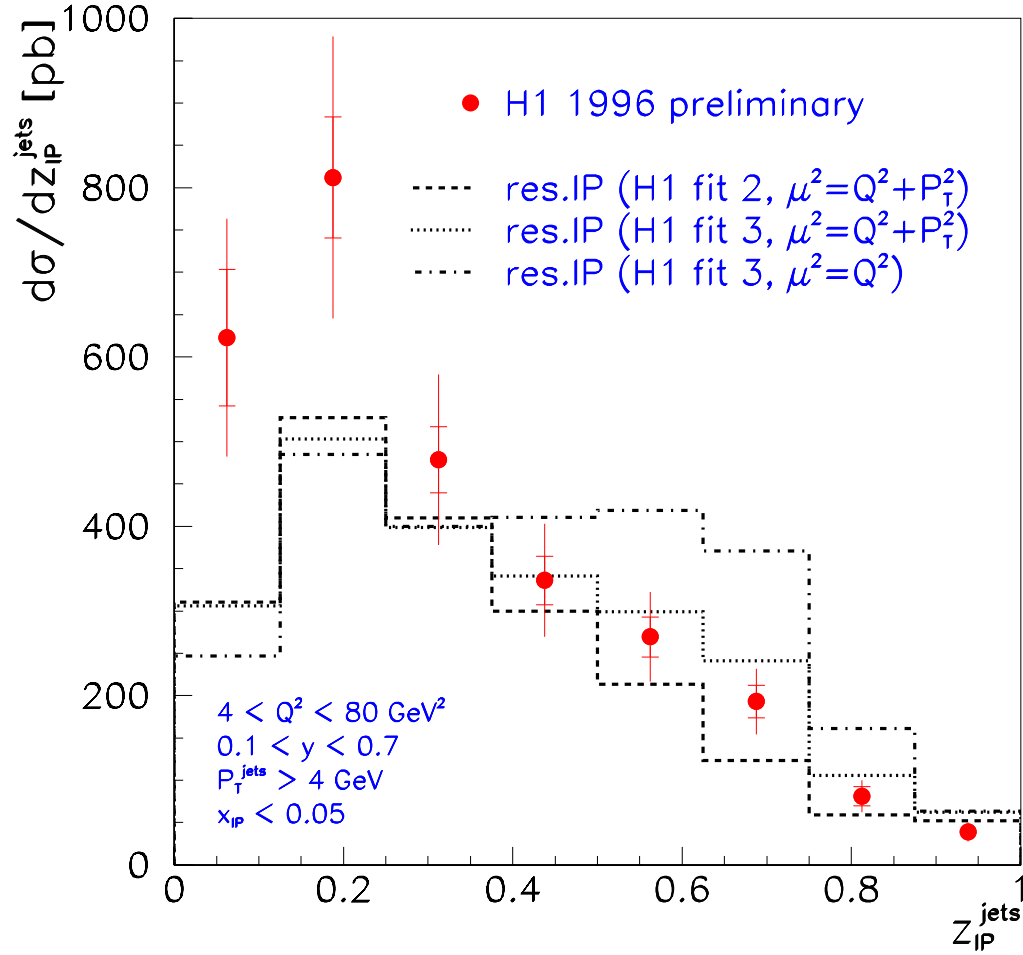
Figure 6: Differential hadron level cross section for diffractive dijet production as a function of an estimator $z_{I\!\!P}^{jets}$ of the momentum fraction of the parton from the pomeron entering the hard scattering process. The data points are shown together with the predictions from a partonic pomeron model, as implemented in the RAPGAP generator with 'flat' (fit 2) and 'peaked' (fit 3) gluon dominated parton densities for the pomeron, evolved to scales $\mu^2 = Q^2$ or $\mu^2 = Q^2 + p_{\mathrm{T}}^2$.
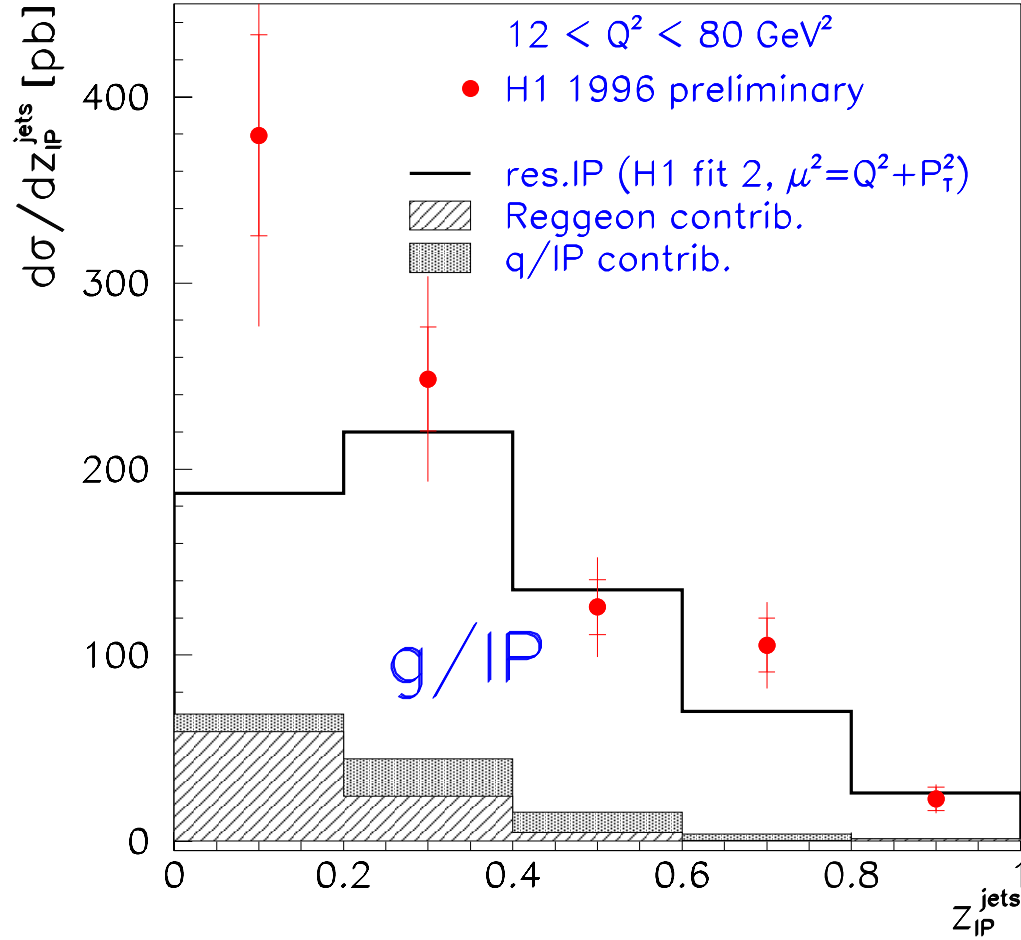
16

Figure 7: Differential hadron level cross section for diffractive dijet production as a function of $z_{I\!P}^{jets}$ for $12 < Q^2 < 80\ \mathrm{GeV}^2$. The data are compared with the prediction of a partonic pomeron model as implemented in the RAPGAP generator ('flat' gluon distribution, $\mu^2 = Q^2 + p_T^2$). The decomposition of the prediction of this model into contributions from subleading reggeon exchange and from quarks and gluons from the pomeron is also shown.
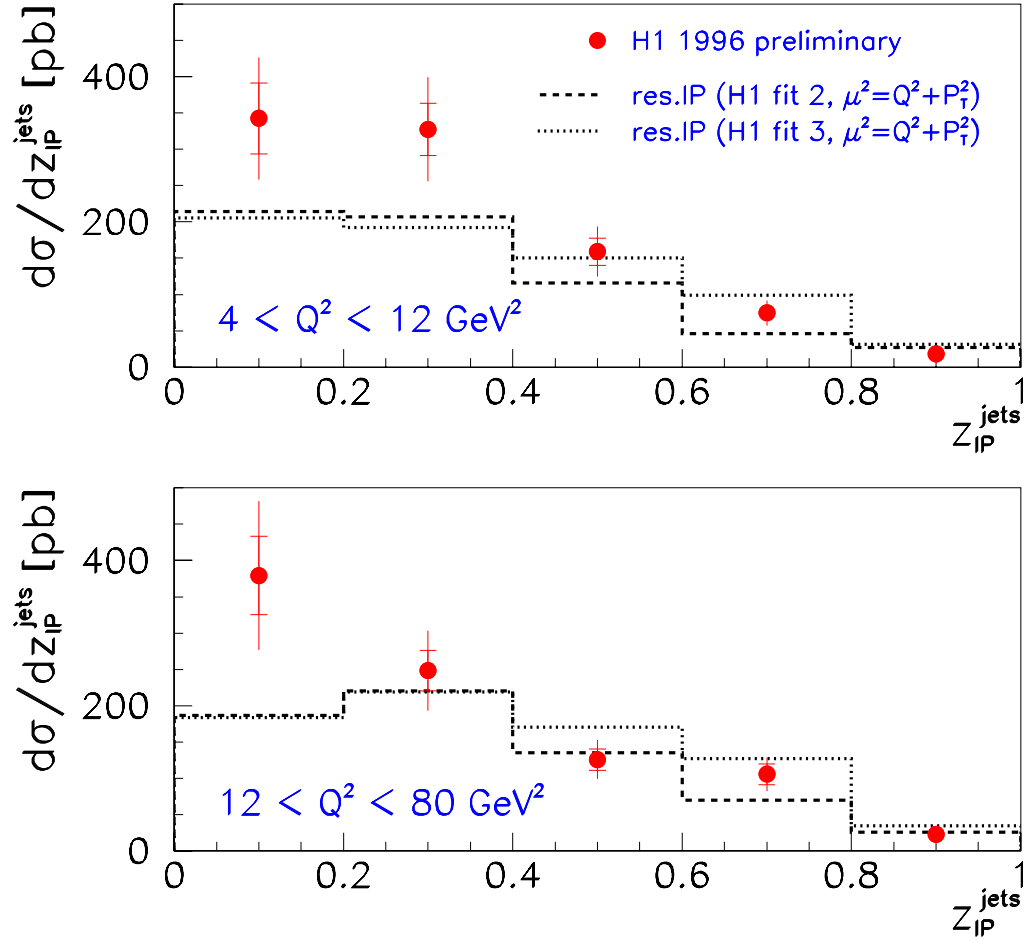
Figure 8: Differential hadron level cross section for diffractive dijet production as a function of $z_{I\!P}^{jets}$, measured in two regions of Q^2. The data are compared to the prediction of a resolved pomeron model, as implemented in the RAPGAP program, with 'flat' (fit 2) and 'peaked' (fit 3) gluon distributions and $\mu^2 = Q^2 + p_{\rm T}^2$.
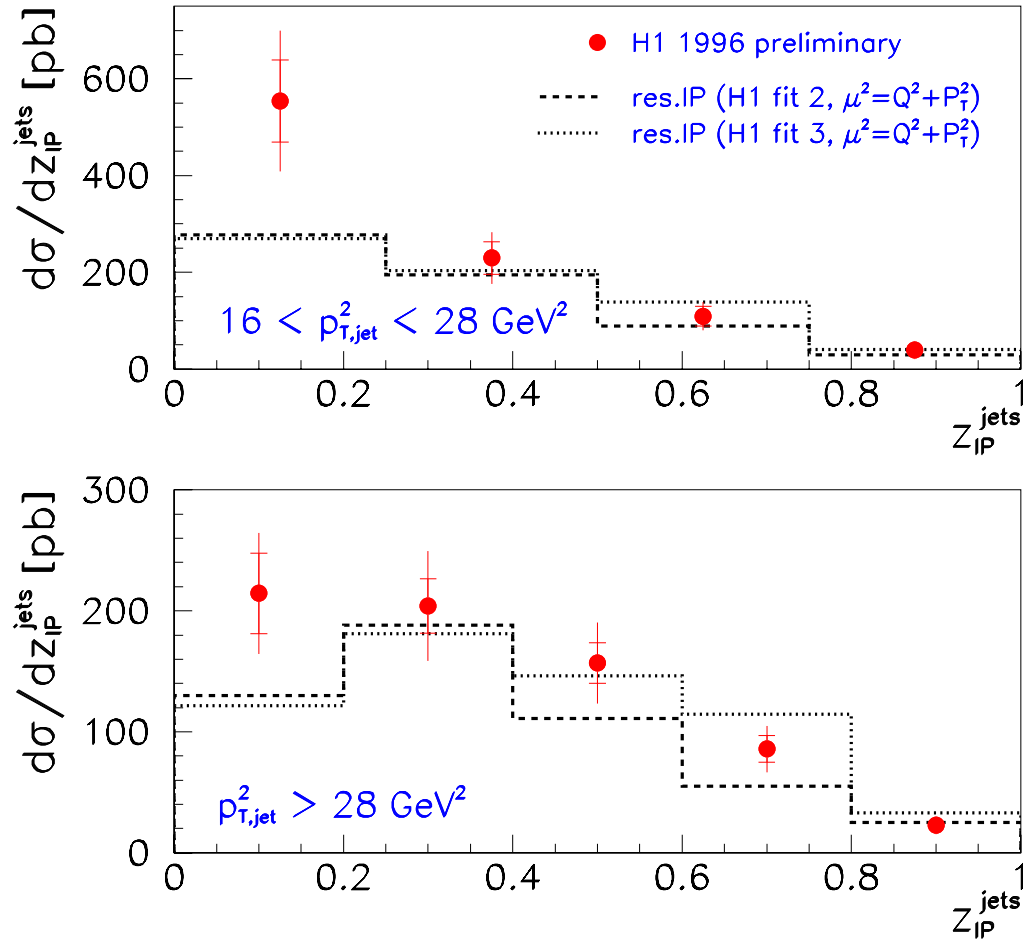
Figure 9: Differential hadron level cross section for diffractive dijet production as a function of $z_{I\!P}^{jets}$, measured in two regions of $p_{T,jet}^2$. The data are compared to the prediction of a resolved pomeron model, as implemented in the RAPGAP program, with 'flat' (fit 2) and 'peaked' (fit 3) gluon distributions and $\mu^2 = Q^2 + p_T^2$.